Birgit Stender*, Oliver Blanck[2], Sebastian D. Reinartz[3], Olaf Dössel[4]

Separating ventricular activity in thoracic EIT using 4D image-based FEM simulations

Abstract: One challenge in central hemodynamic monitoring based on electrical impedance tomography (EIT) is to robustly detect ventricular signal components and the corresponding EIT image region without external monitoring information. Current stimulation and voltage measurement of EIT were simulated with finite element porcine torso models in presence of a multitude of thoracic blood volume shifts. The simulated measurement data was examined for linear dependence on changes in stroke volume. Based on the results the EIT measurement information regarding stroke volume changes is sparse.

Keywords: electrical impedance tomography (EIT), stroke volume (SV), cardiac output (CO), pulmonary artery pressure (PAP), bioimpedance model, finite element method (FEM)

https://doi.org/10.1515/cdbme-2021-2222

1 Introduction

Electrical impedance tomography (EIT) is a real-time capable functional imaging modality which has so far been mainly applied and validated for the monitoring and optimization of regional lung ventilation [1]–[4] and an indicator based assessment of regional lung perfusion [5]–[7]. In addition to respiratory-induced impedance changes, non-invasively measured EIT signals contain as well cardiac-induced signal components of significantly smaller amplitude, which can potentially be utilized for the estimation of central hemodynamic parameters. Monitoring of changes in stroke volume or the diagnosis and classification of pulmonary artery hypertension (PAH) have so far been proposed, for example [8]–[11]. The robust detection of an image region characterized by predominantly ventricular activity is central to both questions. This region is often referred to only as the heart region [11], [12]. In fact, the blood volumes of all four cardiac chambers, the aorta, vena cava, and pulmonary artery change in the course of the cardiac cycle. Therefore, they all potentially cause cardio-synchronous signals in the thoracic EIT signals of different phase.

In preliminary work on the automatic detection of heart and lung image regions in preclinical EIT image time-series, one result was that cardio-synchronous activity can in principle occur in more than just one image region [12]. Ferrario et al partially detected further regions with cardiac induced signals of opposite phase.

The goal of the presented 4D finite element method (FEM) simulation study on EIT was to identify stimulation-measurement electrode pairs that could provide information regarding heart rate and amplitude of the stroke volume (SV) prior to image reconstruction and robustly in presence of subject-specific anatomical variations.

2 Materials

The three porcine torso models underlying the FEM simulation results were created based on a time-series of Computed Tomography (CT) image volumes provided by CyberHeart (Varian Medical Systems, Palo Alto, CA, USA). Only one contrast enhanced CT time-series per animal was provided dedicated to the primary goal of radiation therapy planning in atrial fibrillation. Neither the controlled induction

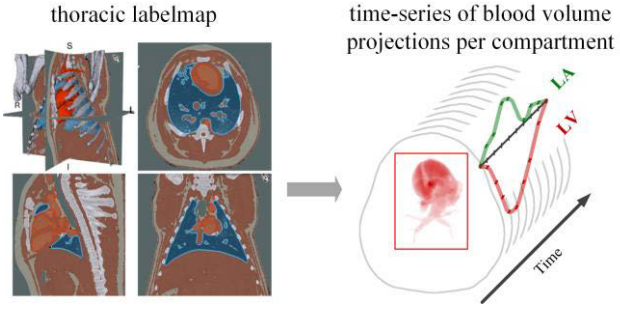

Figure 1: Workflow for the generation of reference time-series in each of the three cardiac CT datasets.

***Corresponding author: Birgit Stender:** Drägerwerk AG & Co. KGaA, Lübeck, Germany, e-mail: birgit.stender@draeger.com, [2]Radiation Therapy, University Medical Center Schleswig-Holstein, Kiel, Germany, [3]Department of Diagnostic and Interventional Radiology, University Hospital, RWTH Aachen University, Aachen, Germany, [4]Institute of Biomedical Engineering, KIT, Karlsruhe, Germany

of SV changes nor repetitive imaging in randomly deviating cardiovascular states were part of the protocol.
The images were recorded with a LigthSpeed^{TM} VCT Scanner (GE Healthcare, Chalfont St Giles, GB). Each time-series included ten frames taken with 227 ms exposure time, 1.25 mm slice thickness and a pixel spacing of 0.64 x 0.64 mm. The female pigs under anesthesia were pressure controlled ventilated. The cardiac CT scanning was gated based on an electrocardiogram (ECG) during a breath-holding maneuver after giving a bolus of contrast agent intravenously.
To be consistent to the porcine anatomy, an EIT image reconstruction method was trained on dual-energy CT (DECT) image data of thirteen animals from a second preclinical trial. These images were recorded as part of validation study on regional ventilation in EIT. Please refer to Reinartz et al regarding the animal preparation, protocol and details of the DECT imaging system, [3]. The image data used for training of the EIT image reconstruction was selected from one distinct lung state at a positive end-expiratory pressure (PEEP) of 15 mbar.

3 Methods

3.1 Set-up of the FEM torso models

The thoracic blood volume pool as well as other tissue types were segmented from contrast enhanced 4D cardiac CT time-series based on thresholding and morphological operations. The skeletal bone structure was used to initially align and co-register the image volumes. An exemplary segmentation result is shown on the left part of **Figure 1**. The contribution of each compartment to the time-series of 1D/2D volume projections was determined as illustrated on the right.
For volume mesh generation triangulated surface models were created as isosurfaces at the labelmap resolution of (1 x 1 x 1 mm). The torso surface is shown in **Figure 2**. at the left hand-side. It is displayed in conjunction with the sixteen electrode surface meshes prior to their integration into the torso surface mesh. The electrodes were positioned along an axial circumferential line 1 cm inferior of the common end-diastolic ventricular blood volume centroid. The torso surface mesh including the complex electrode surfaces was supplemented by interior isosurfaces generated from the labels of bone and blood. The density of the compound tetrahedral volume mesh was controlled by a combination of the compound surface mesh densities in combination with a constrained on the maximum tetrahedral volume (25 mm^3). The volume mesh was created for each point in time individually.

Figure 2: On the left: 2D electrode surface meshes in their positions prior to ray-tracing for final placement. On the right: Isosurface meshes underlying the volume mesh generation

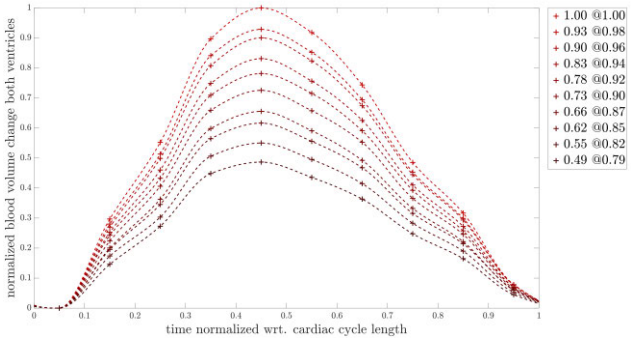

Figure 3: Effect of uniform scaling regarding the relative change in common ventricular stroke volume within the first (reference) animal data set.

To assess the influence of SV variations on EIT measurements, reductions of the initial SV were geometrically modelled. Nine different parametrizations of a rigid transformation were applied to the originally segmented left ventricular (LV) and right ventricular (RV) volumes, given as binary mask volumes. Reference point for these transformations was the common centroid of both volumes at the original common end-diastolic state. The spatial transformations applied were represented by a uniform scaling with a scaling factor in the range between 0.98 and 0.79. The effect on the common ventricular volume trace and the SV of both ventricles is shown in **Figure 3**. The scaling resulted in a stepwise reduction of up to 49 % in both the common end-diastolic ventricular volume and the SV. Voxels, which were part of the originally segmented LV and RV blood volumes, but not included in their transformed binary masks, were assigned to (myocardial) muscle in the corresponding thoracic labelmap volume.

Surface meshing, mesh integrity checking, remeshing and tetrahedral volume meshing with TETGEN were included in a meshing pipeline implemented in Matlab [13], [14]. For tissue types other than lung parenchyma, conductivity values were assigned according to Gabriel and Gabriel at the stimulation frequency of 100 kHz [15], [16]. The solutions of

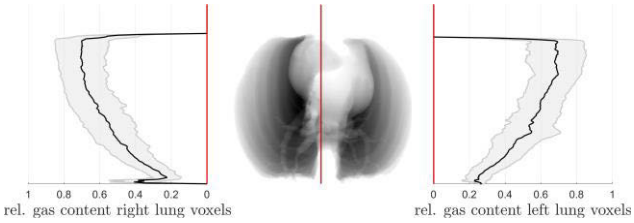

Figure 4: Pulmonary inhomogeneity in mean voxel alveolar air content V_A for the first (reference) animal data set at a specific position in dorsal-ventral direction. The gray filled areas displayed in the background of the mean projection trace are spanned by the voxel mean ± standard deviation at the respective position in dorsal-ventral direction.

the complete electrode model (CEM) of the torso in adjacent stimulation and measurement mode were computed with the standard solver in EIDORS [17].

3.2 Pulmonary background impedance

The dielectric properties of a lung parenchyma strongly depend on the regional alveolar air volume V_A, which is known to be spatially inhomogeneous for a variety of reasons, among them are gravitational effects [18]. In **Figure 4** the inhomogeneity of V_A is shown for the first (reference) animal data set. The projections in cranial-caudal direction were derived based on the CT numbers (Hounsfield Units) of the voxels contained within the lung mask. Evaluating the model of Nopp et al. at the given stimulation frequency and the regional relative proportion of V_A, a pulmonary conductivity distribution with strong dorsal-ventral gradient was included in the torso forward models [19], [20].

3.3 Image reconstruction

For EIT image reconstruction a 64 x 64 element normalized time-difference (NTD) Graz consensus reconstruction algorithm for EIT (GREIT) was trained [21]. The noise figure was fixed (NF = 0.5). It is well known that a more homogeneous sensitivity distribution for EIT time difference imaging can be achieved for impedance changes within the lung region by taking into account the actually inhomogeneous thoracic background impedance distribution as well as the lung asymmetry that results from the enclosure of the pericardium [22]. Since these conclusions can presumably be extended to the signal amplification within the epicardium, a realistic median 3D thoracic conductivity distribution was used in the training process. It was derived based on co-registered DECT image scans in 13 animals. The figures of merit were determined for 500 target positions uniformly distributed in axial slices and within the interval [-5 cm , +5 cm] in cranio-caudal direction with respect to the electrode plane.

4 Results

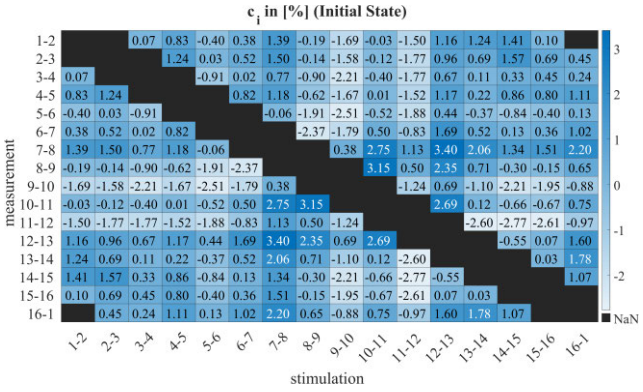

Figure 5: Matrix containing the weights c_i determined for the initial (maximum) stroke volume without applying a scaling factor.

The normalized common ventricular volume trace was regarded as signal component potentially present in each time-series of the normalized voltages. The weights c_i were computed as

$$\underset{c_i}{\mathbf{argmin}} \sum_{k=1}^{nT} \left(v_{n,i}(k) - c_i \cdot \Delta V_{ventricles,n}(k) \right)^2, \qquad (1)$$

where $\Delta V_{ventricles,n}(k)$ denotes one of the $nT = 10$ samples of the normalized ventricular volume trace and $v_{n,i}(k)$ a sample of one the $i = 1, \ldots, 208$ NTD voltage time-series. Exemplary results are shown in **Figure 5** for the initial hemodynamic state in the first torso model.

Selected were stimulation-measurement pairs exceeding a Pearson correlation of 0.75 between the absolute stroke volumes and the weights c_i based on the simulation results in each of the torso models. This selection criterion resulted in a reduction to just eight measurement time-series further regarded. The current paths for the identified stimulation-measurement combinations run mostly through the ventral part of the right lung and are not the ones characterized by the largest values in c_i. For all 30 reconstructed EIT image time-series, a ventrally located simply connected image region with cardio-synchronous activity became much more clearly visible. An example is shown in **Figure 6**. The entire image signal of this image time-series showed a high linear

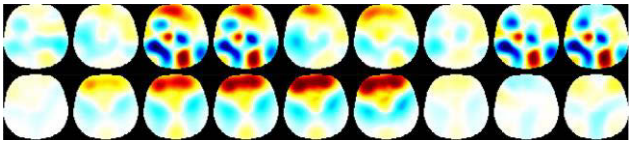

Figure 6: Cardiac EIT time-series reconstructed for the initial SV in the first (reference) animal with 208 (top row) and the selected eight voltage measurements (bottom row). The underlying voltage time-series included $nT = 10$ samples. The initial set of measurement voltages defined the reference for normalization.

dependence on the course of the common ventricular blood volume trace.

5 Discussion and Conclusion

The presented work could be extended in some aspects. The changes in the end-diastolic ventricular blood volume and the stroke volume were modelled by isolated geometric scaling and in direct exchange between ventricular blood volume and myocardial volume. Neither the effects of preload changes nor mechanical heart-lung interactions were addressed so far. Pulsatility signals from blood volume pulses propagating in the smaller vessels within the pulmonary circulations were not regarded as well. Nevertheless, seven different larger compartments contributing to cardio-synchronous signals were included in the investigation. The presented GREIT reconstruction model differs from previously presented human and porcine GREIT reconstruction models, because the forward model used in the training process was not derived just as an extrusion based on a single axial image slice but from real 3D imaging data in a larger number of animals.

However, the effects of background impedance changes on the amplitude of the ventricular induced EIT signals need to be investigated in more detail. The observed improvement in the separation of the ventricular image region through the presented selection of the measured values prior to the actual reconstruction should be further examined on pre-clinical measurement data sets in different lung and hemodynamic conditions including stroke volume reference data.

Author Statement

Research funding: The author state no funding beyond the use of the DECT imaging data. Conflict of interest: Birgit Stender is an employee of medical device manufacturer Dräger. The other authors state no conflict of interest. Ethical approval: The local animal care committees approved the two animal studies providing the underlying image data basis.

References

[1] E. L. V Costa *et al.*, “Bedside estimation of recruitable alveolar collapse and hyperdistension by electrical impedance tomography,” *Intensive Care Med.*, vol. 35, pp. 1132–1137, 2009.

[2] C. Gomez-Laberge, J. H. Arnold, and G. K. Wolf, “A unified approach for EIT imaging of regional overdistension and atelectasis in acute lung injury,” *IEEE Trans. Med. Imaging*, vol. 31, no. 3, pp. 834–842, 2012.

[3] S. D. Reinartz *et al.*, “EIT monitors valid and robust regional ventilation distribution in pathologic ventilation states in porcine study using differential DualEnergy-CT (ΔDECT),” *Sci. Rep.*, vol. 9, no. 1, pp. 1–10, 2019.

[4] P. Davies, S. Yasin, S. Gates, D. Bird, and C. Silvestre, “Clinical Scenarios of the Application of Electrical Impedance Tomography in Paediatric Intensive Care,” *Sci. Rep.*, vol. 9, no. 1, pp. 1–8, 2019.

[5] J. B. Borges *et al.*, “Regional lung perfusion estimated by electrical impedance tomography in a piglet model of lung collapse,” *J. Appl. Physiol.*, vol. 112, no. 1, pp. 225–236, Jan. 2012.

[6] T. Bluth *et al.*, “Measurement of relative lung perfusion with electrical impedance and positron emission tomography: an experimental comparative study,” *Br. J. Anaesth.*, vol. 123, no. May, pp. 246–254, 2019.

[7] M. Kircher *et al.*, “Regional Lung Perfusion Analysis in Experimental ARDS by Electrical Impedance and Computed Tomography,” *IEEE Trans. Med. Imaging*, vol. 40, no. 1, pp. 251–261, 2021.

[8] R. Pikkemaat, S. Lundin, O. Stenqvist, R.-D. Hilgers, and S. Leonhardt, “Recent Advances in and Limitations of Cardiac Output Monitoring by Means of Electrical Impedance Tomography,” *Anesth. Analg.*, vol. 119, no. 1, pp. 76–83, 2014.

[9] M. Proença, F. Braun, J. Solà, J. P. Thiran, and M. Lemay, “Noninvasive pulmonary artery pressure monitoring by EIT: a model-based feasibility study,” *Med. Biol. Eng. Comput.*, vol. 55, no. 6, pp. 949–963, 2017.

[10] F. Braun *et al.*, “Limitations and Challenges of EIT-Based Monitoring of Stroke Volume and Pulmonary Artery Pressure,” *Physiol. Meas.*, pp. 1–25, 2017.

[11] F. Braun, M. Proença, A. Adler, T. Riedel, J.-P. Thiran, and J. Solà, “Accuracy and reliability of noninvasive stroke volume monitoring via ECG-gated 3D electrical impedance tomography in healthy volunteers,” *PLoS One*, vol. 13, no. 1, p. e0191870, 2018.

[12] D. Ferrario, B. Grychtol, A. Adler, J. Solà, S. H. Böhm, and M. Bodenstein, “Towards morphological thoracic EIT: Major signal sources correspond to respective organ locations in CT,” *IEEE Trans. Biomed. Eng.*, vol. 59, no. 11, pp. 3000–3008, 2012.

[13] Q. Fang, “iso2mesh: a matlab-based 3D tetrahedral mesh generator,” 2008. [Online]. Available: http://iso2mesh.sourceforge.net.

[14] H. Si, “TetGen, a Delaunay-Based Quality Tetrahedral Mesh Generator,” *ACM Trans. Math. Softw.*, vol. 41, no. 2, p. Article No.: 11, 2015.

[15] C. Gabriel, S. Gabriel, and E. Corthout, “The dielectric properties of biological tissues: I. Literature survey,” *Phys. Med. Biol.*, vol. 41, no. 11, pp. 2231–2249, 1996.

[16] C. Gabriel, a Peyman, and E. H. Grant, “Electrical conductivity of tissue at frequencies below 1 MHz.,” *Phys. Med. Biol.*, vol. 54, no. 16, pp. 4863–4878, 2009.

[17] A. Adler and W. R. B. Lionheart, “Uses and abuses of EIDORS: an extensible software base for EIT,” *Physiol. Meas.*, vol. 27, no. 5, pp. 25–42, 2005.

[18] I. Galvin, G. B. Drummond, and M. Nirmalan, “Distribution of blood flow and ventilation in the lung: Gravity is not the only factor,” *Br. J. Anaesth.*, vol. 98, no. 4, pp. 420–428, 2007.

[19] P. Nopp, E. Rapp, H. Pfützner, H. Nakesch, and C. Ruhsam, “Dielectric properties of lung tissue as a function of air content,” *Phys. Med. Biol.*, vol. 38, no. 6, pp. 699–716, 1993.

[20] P. Nopp, N. D. Harris, T. X. Zhao, and B. H. Brown, “Model for the dielectric properties of human lung tissue against frequency and air content,” *Med. Biol. Eng. Comput.*, vol. 35, no. 6, pp. 695–702, 1997.

[21] A. Adler *et al.*, “GREIT: A unified approach to 2D linear EIT reconstruction of lung images,” *Physiol. Meas.*, vol. 30, no. 6, 2009.

[22] B. Grychtol and A. Adler, “Uniform background assumption produces misleading lung EIT images,” *Physiol. Meas.*, vol. 34, no. 6, pp. 579–593, 2013.